ARMA 19-1619

Propagation of a planar hydraulic fracture perpendicular to the isotropy plane of a transversely isotropic material

Moukhtari, F.E.
EPFL, Lausanne, Switzerland
Lecampion, B.
EPFL, Lausanne, Switzerland
Zia, H.
EPFL, Lausanne, Switzerland

ABSTRACT: We investigate the case of a hydraulic fracture (HF) propagating perpendicular to the isotropy plane of a transversely isotropic material: a relevant configuration for the growth of HFs in sedimentary rocks where fractures are propagating vertically across layers. We extend the implicit level set algorithm originally developed for the propagation of planar 3D HF in isotropic media to transverse isotropy (TI) of elasticity and toughness. Contrary to the isotropic case, the near-tip plane strain elastic relation depends on the angle α between the local propagation direction and the isotropy plane. We present an analytical solution for an elliptical HF in the toughness dominated regime and use it to benchmark our numerical solver. For a TI elastic material, we investigate HF growth for two different assumptions: isotropic material toughness or isotropic critical fracture energy. In both cases, we compare the fracture aspect ratio obtained by our numerical results with simplified estimations based on the minimization of the variation of local stress intensity factor (or energy release rate) under the assumption of an elliptical fracture. Our numerical results show that for both assumptions, the fracture aspect ratio inversely scales with the ratio of plane-strain elastic modulus in the two orthogonal directions of the material frame with a different exponent. However, the fracture is never strictly elliptical, except for a very peculiar form of toughness anisotropy.

1. INTRODUCTION

A number of sedimentary rocks are composed of beds of metric to sub-metric scales. Such a lamination intrinsic to the rock diagenesis leads to a transverse isotropy. The effect of such type of anisotropy on the propagation of hydraulic fracture remains poorly understood, and most hydraulic fracturing models assume isotropic elasticity. Hydraulic fracture propagation is governed by strong couplings between rock deformation, fracturing and viscous flow within the newly created fracture (Detournay, 2016). The goal of this study is to investigate the effect of transverse isotropy on HF growth focusing on the case of a planar fracture propagating perpendicular to the isotropy plane (Fig. 1). We restrict to an impermeable media and a Newtonian fluid.

2. PROBLEM FORMULATION

We study the case of a planar hydraulic fracture (HF) propagating in transverse isotropic (TI) impermeable media. We introduce the material canonical orthonormal basis (e_1, e_2, e_3) where e_3 is the axis of symmetry and (e_1, e_2) is the plane of material isotropy. The TI stiffness matrix c_{ijkl} can be expressed in terms of the five parameters $(C_{11}, C_{12}, C_{13}, C_{33}, C_{44})$ in Voigt notation (see e.g. Pan and Chou (1976); Voigt (1928)).We focus on the case of a hydraulic fracture propagating in the (e_1, e_3) plane perpendicular to the plane of isotropy. The fracture is subject to an internal fluid pressure p_f (function of space and time) and an external uniform far field stress σ_h. The fracture is driven by the injection of a Newtonian fluid (viscosity μ) under a constant rate Q_o from a point source.

2.1. Governing equations

Under the configuration of Fig. 1, the planar HF exhibit pure mode I (see Keer and Lin (1990); Lin and Keer (1989)), the net pressure $p(\boldsymbol{y}) = p_f(\boldsymbol{y}) - \sigma_h$ at $\boldsymbol{y} \in (e_1, e_3)$ is related to the normal displacement discontinuity profile $w(\boldsymbol{x})$ via the following boundary integral equation (see e.g. Bonnet (1999); Mogilevskaya (2014)):

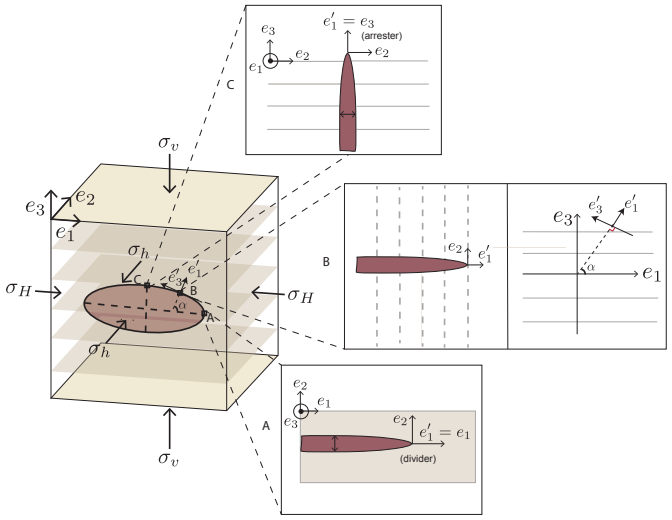

Fig. 1: Schematic of planar hydraulic fracture perpendicular to the plane of material isotropy normal to the in-situ minimum stress. The different configurations of the region near tip around the fracture front is also reported: (A) semi- infinite fracture propagating along the divider direction, (B) semi-infinite fracture propagating within the plane (e_1, e_3) and (C) semi-infinite fracture propagating along the arrester direction.

$$p_f(\boldsymbol{y}) - \sigma_h = c_{22mn} \int_\Sigma S^m_{k2}(\boldsymbol{y},\boldsymbol{x}) \big(\delta_{2n} \frac{\partial w}{\partial x_k}(\boldsymbol{x}) - \delta_{2k} \frac{\partial w}{\partial x_n}(\boldsymbol{x})\big) \mathrm{d}x_1 \mathrm{d}x_3, \quad (1)$$

where $S^m_{ij}(\boldsymbol{y},\boldsymbol{x})$ is the stress tensor at point x due to an unit force at y in the m direction. δ_{ij} is the Kronecker delta operator.

Under the assumption of an incompressible fluid, the width averaged fluid mass equation reduce to the following continuity equation when neglecting any fluid leak-off:

$$\frac{\partial w}{\partial t} + \nabla \boldsymbol{q} = Q_o \delta(x_1, x_3) \quad (2)$$

Under lubrication flow, the fluid flux $\boldsymbol{q}$ is related to the fluid pressure gradient and opening via Poiseuille's law:

$$\boldsymbol{q} = -\frac{w^3}{\mu'} \boldsymbol{\nabla} p_f \quad (3)$$

where $\mu' = 12\mu$.

2.2. Boundary conditions

For sufficiently deep fractures, the fluid lag is negligible leading to the following boundary conditions along the fracture front $\mathscr{C}(t)$ (Detournay, 2016):

$$w(\boldsymbol{x}_{\mathscr{C}}, t) = 0,\ \boldsymbol{q}(\boldsymbol{x}_{\mathscr{C}}, t) = 0,\ \boldsymbol{x}_{\mathscr{C}} \in \mathscr{C}(t). \quad (4)$$

We investigate the general case when both the material elasticity and the fracture toughness are anisotropic with respect to the TI configuration. The fracture toughness, thus, depends on the local fracture propagation direction, namely the angle α. The angle α is defined as the angle between the local propagation direction (normal to the tangent of the fracture front) and the divider direction e_1 (see Fig. 1).

For a pure mode I fracture, the quasi-static propagation condition along the fracture front can be either written in terms of energy release rate or stress intensity factor thanks to Irwin's relation (see Stroh (1958); Barnett and Asaro (1972) for the anisotropic case) - using the later here-, we write

$$K_I(\boldsymbol{x}_{\mathscr{C}}, t) = K_{Ic}(\alpha),\ \boldsymbol{x}_{\mathscr{C}} \in \mathscr{C}(t) \quad (5)$$

where the material fracture toughness K_{Ic} may be function of the fracture propagation direction - here the angle α between the local propagation direction and the e_1 axis of the material frame.

2.3. Near Tip Elastic behavior

The near-tip region of a hydraulic fracture is where the fluid-solid coupling non-linearities of the problem resides - and as such are well known to control the finite hydraulic fracture growth behavior for isotropic material (Garagash, 2009).

It is possible to derive a near-tip plane-strain operator for a mode I semi-infinite HF propagating at an angle α with respect to the divider direction e_1 (see Fig. 1). Such a configuration is a local zoom into the tip region - now function of the propagation direction due to material anisotropy. We define the local axis e_1' of the direction of propagation of the semi-infinite fracture where $\widehat{(e_1', e_1)} \equiv \alpha$, and $e_2' = e_2$ is the normal to the fracture surface. A near tip elastic deformation can be then derived from the solution of an edge dislocation in anisotropic media (Hirth and Lothe, 1982):

$$p(y_1') = p_f(y_1') - \sigma_h = \frac{E'_\alpha}{4\pi} \int_0^\infty \frac{1}{y_1' - x_1'} \frac{\partial w}{\partial x_1'} dx_1', \quad (6)$$

where E'_α is a near tip plane-strain anisotropic elastic modulus which depends obviously on the propagation direction (via angle α) as well as all the elastic constants C_{ij}. E'_α can be expressed function of a dimensionless function F as

$$E'_\alpha = \langle E' \rangle \times F(\alpha, \beta, \varepsilon, \delta, C_{13}/C_{11}) \quad (7)$$

where the elastic mean value $\langle E' \rangle$, the anisotropy ratio β, and Thomson parameters $\{\delta, \varepsilon\}$ are given as:

$$\begin{cases} \langle E' \rangle = & \dfrac{E'_\alpha(\alpha=0)+E'_\alpha\left(\alpha=\frac{\pi}{2}\right)}{2} \\ \beta = & \dfrac{E'_\alpha(\alpha=0)}{E'_\alpha\left(\alpha=\frac{\pi}{2}\right)} \\ \varepsilon = & (C_{11}-C_{33})/(2C_{33}) \\ \delta = & \dfrac{(C_{13}+C_{44})^2-(C_{33}-C_{44})^2}{2C_{33}(C_{33}-C_{44})} \end{cases} \tag{8}$$

It is important to note that the near-tip plane-strain operator (6) has a form strictly equal to the isotropic case pending the use of modulus E'_α. As a result, all the hydraulic fracture tip asymptotes obtained for the isotropic case can be chiefly used in anisotropy pending the proper use of E'_α. Notably, very near the tip, the linear elastic fracture mechanics asymptote prevails, i.e.

$$w = \sqrt{\frac{32}{\pi}}\frac{K_{Ic}}{E'_\alpha}\sqrt{\rho} \qquad \rho \ll 1 \tag{9}$$

where ρ is the closest distance to the fracture front in the propagation direction.

In the isotropic case, the modulus E'_α simply reduces to the plain strain Young's modulus $E' = C_{11}\left(1-\frac{C_{12}^2}{C_{11}^2}\right)$. We do not report here the analytical expression of E'_α as it is quite lengthly. We plot in Fig. 2 the scaled anisotropic modulus $E'_\alpha/\langle E' \rangle$ as function of the angle α for different values of the dimensionless parameters $\{\beta, \varepsilon, \delta, C_{13}/C_{11}\}$. The magnitude of the elastic modulus is controlled by the ratio β, whereas, the slope is function of $\{\beta, \varepsilon, C_{13}/C_{11}\}$. The Thomson parameter δ has a second order effect on the variation of E'_α. We also compare the analytical expression (solid lines) to the approximation function $E'_{app}/\langle E' \rangle$ proposed by Laubie and Ulm (2014) (dashed line):

$$\frac{1}{E'_{app}} = \frac{\cos^2(\alpha)}{E'_\alpha(\alpha=0)} + \frac{\sin^2(\alpha)}{E'_\alpha\left(\alpha=\frac{\pi}{2}\right)} \tag{10}$$

This approximation underestimates in most cases the exact expression of E'_α, and is only valid for a low degree of anisotropy (i.e. for $\beta < 1.5$) (see Fig. 2). For simplicity, we will focus thereafter only on the effect of the anisotropic elastic ratio β while we will set the other parameters to the following values: $\varepsilon = 0.3$, $\delta = 0.2$, and $C_{13}/C_{11} = 0.5$ in the remainder of this paper.

3. DIMENSIONAL ANALYSIS AND SCALING

The propagation of HF fracture in impermeable media is governed by two distinct regimes: toughness and viscosity (Detournay, 2016). In the following, we focus only on the toughness dominated regime which dominates at large injection time when the effect of the fracture energy becomes larger than viscous fluid dissipation. Following Savitski and

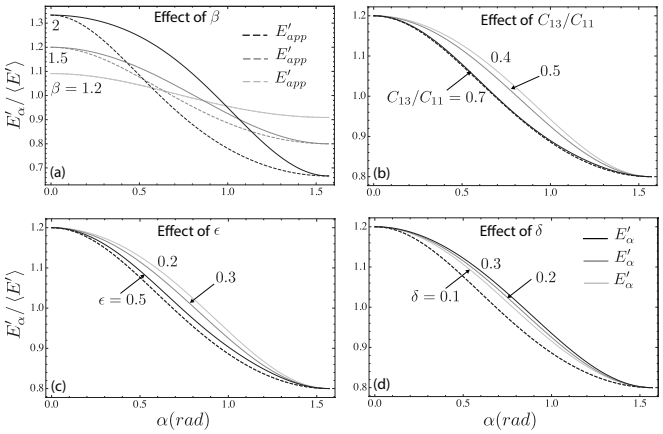

Fig. 2: Near tip plane strain modulus E'_α as function of the propagation direction angle α. Exact solution (solid lines) and the approximation used in Laubie and Ulm (2014) (dashed line). Influence of the different dimensionless elastic constants: (a) effect of $\beta = \{1.2, 1.5, 2\}$ for $\varepsilon = 0.3$, $\delta = 0.2$, and $C_{13}/C_{11} = 0.5$, (b) effect of $C_{13}/C_{11} = \{0.4, 0.5, 0.7\}$ for $\beta = 1.5$, $\varepsilon = 0.3$, and $\delta = 0.2$, (c) effect of $\varepsilon = \{0.2, 0.3, 0.5\}$ for $\beta = 1.5$, $\delta = 0.2$, and $C_{13}/C_{11} = 0.5$, and (d) effect of $\delta = \{0.1, 0.2, 0.3\}$ for $\beta = 1.5$, $\varepsilon = 0.3$, and $C_{13}/C_{11} = 0.5$.

$L_k(t)$	$\left(\dfrac{\langle E' \rangle Q_o t}{\sqrt{\frac{32}{\pi}}\langle K_{Ic} \rangle}\right)^{2/5}$
$W_k(t)$	$\left(\dfrac{Q_o\left(\sqrt{\frac{32}{\pi}}\langle K_{Ic} \rangle\right)^4 t}{\langle E' \rangle^4}\right)^{1/5}$
$P_k(t)$	$\left(\dfrac{\left(\sqrt{\frac{32}{\pi}}\langle K_{Ic} \rangle\right)^6}{Q_o \langle E' \rangle t}\right)^{1/5}$

Table 1: Characteristic lengthscales in the toughness dominated scaling.

Detournay (2002); Madyarova and Detournay (2003), we use the so-called toughness dominated scaling. We scale the dimensional unknowns: fracture front, width and pressure by the characteristic lengthscales $L_k(t)$, $W_k(t)$, and $P_k(t)$ respectively (see Table 1). We choose the scaling toughness as the mean value $\langle K_{Ic} \rangle = \dfrac{K_{Ic}(\alpha=0)+K_{Ic}\left(\alpha=\frac{\pi}{2}\right)}{2}$.

4. ELLIPTICAL HF TOUGHNESS DOMINATED SOLUTION

We derive here the solution for a propagating toughness dominated elliptical HF. In the toughness dominated, the net pressure is spatially uniform.

For an elliptical fracture of semi-major axis a and semi-minor axis b subject to an uniform pressure p in an infinite medium, following Eshelby *et al.* (1953) the corresponding

fracture opening takes the given form:

$$w = w_0 p\sqrt{ab}\sqrt{1-\frac{x_1^2}{a^2}-\frac{x_3^2}{b^2}} \tag{11}$$

where w_0 is an pre-factor that needs to be determined. We will follow here the approach described by Hoenig (1978) to obtain such pre-factor. First, using the geometrical properties of the ellipse we show that near tip the first order term of the fracture opening is simplified to (Hills *et al.*, 1996):

$$w = w_0 p\sqrt{a}\sqrt{2\rho}\left(\sin^2\theta+\gamma^2\cos^2\theta\right)^{1/4} \tag{12}$$

where ρ is the minimum distance between a point inside the elliptical fracture and its closest projection on the fracture front, $\gamma = b/a < 1$ is the fracture aspect ratio, and θ refers to:

$$\theta = \arctan\left(\gamma\tan\alpha\right). \tag{13}$$

We obtain the expression of the stress intensity factor by equalizing the tip asymptote (Eq. (9)) and taking the limit of Eq. (12) for small ρ

$$K_I = \frac{w_0}{4}\sqrt{\pi a}E'_\alpha p\left(\sin^2\theta+\gamma^2\cos^2\theta\right)^{1/4} \tag{14}$$

On the other hand, the global energy release rate G is obtained from the work W applied by the uniform pressure as:

$$G = \frac{1}{2\pi\gamma a}\frac{\partial W}{\partial a} = \frac{1}{2\pi\gamma a}\frac{\partial}{\partial a}\left(\frac{1}{2}pV_{frac}\right) = \frac{1}{2}p^2\gamma^{1/2}aw_0, \tag{15}$$

where V_{frac} is the fracture volume.

The global energy is also equal to the integral of the local energy release rate along the fracture front:

$$G = \frac{1}{2\pi}\int_0^{2\pi} g\mathrm{d}\theta, \tag{16}$$

where g is given by the local stress intensity factor and the near tip anisotropic modulus via:

$$g = \frac{K_I^2}{E'_\alpha} \tag{17}$$

Equalizing the two expression of the global energy release rate (15) and (16), we find the opening magnitude w_0:

$$w_0 = 16\gamma^{1/2}\frac{1}{\int_0^{2\pi}E'_\alpha\left(\gamma^2\cos[\theta]^2+\sin[\theta]^2\right)^{1/2}\mathrm{d}\theta}. \tag{18}$$

For the isotropic elastic case, w_0 can be obtained completely analytically function of the complete elliptical integral of the second kind $\mathbb{E}\left(\sqrt{1-\gamma^2}\right)$.

$$w_{0,iso} = \frac{4}{\langle E'\rangle\,\mathbb{E}\left(\sqrt{1-\gamma^2}\right)}\gamma^{1/2} \tag{19}$$

It is interesting to note that this problem has also been investigated by Fabrikant (2011); Kanaun (2007) recently. However, their analytical solutions contain some errors and do not match with the one obtained from the procedure outlined above - originally derived by Hoenig (1978). Note that the solution reported here matches exactly finite element results.

For a self similar growth, the SIF should be equal to the material fracture toughness at all points along the front: ($K_I = K_{Ic}$). This therefore imply a particular form of material fracture toughness variation with angle which must be of the form of Eq. (20). Introducing $K_{Ic,3}$ as the material toughness in the divider direction e_3 (and E'_3 the corresponding plane-strain modulus), we obtain the following fracture toughness anisotropic function in order to strictly ensure an elliptical fracture

$$K_{Ic} = K_{Ic,3}\left(\frac{E'\alpha}{E'_3}\right)\left(\sin^2\theta+\gamma^2\cos^2\theta\right)^{1/4} \tag{20}$$

Denoting $\kappa = K_{Ic,1}/K_{Ic,3}$ as the toughness ratio between the arrester and divider directions, the fracture aspect ratio γ is given by:

$$\gamma = \left(\frac{K_{Ic,1}}{K_{Ic,3}}\frac{E'_3}{E'_1}\right)^2 = \left(\frac{\kappa}{\beta}\right)^2 \tag{21}$$

We can then obtain the following expression for the net pressure combining Eqs. (14) and (20):

$$p(t) = \frac{4K_{Ic,3}}{w_0E'_3\sqrt{\pi\gamma b(t)}}. \tag{22}$$

and using the volume balance (equivalence of injected volume and fracture volume), we derive the following propagation solution (e.g. Zia *et al.* (2018)):

$$b(t) = \left(\frac{3tQ_oE'_3}{8K_{Ic,3}\sqrt{\pi}}\gamma\right)^{2/5}, \quad a(t) = \left(\frac{K_{Ic,3}}{K_{Ic,1}}\frac{E'_1}{E'_3}\right)^2 b(t). \tag{23}$$

Such a toughness dominated TI elliptical HF growth solution is obviously self-similar like the radial hydraulic fracture for isotropic material.

5. NUMERICAL SCHEME

We discretize the fracture plane with rectangular element and track the fracture front using a level set - following the implicit level set algorithm introduced by Peirce and Detournay (2008). Piece-wise constant displacement discontinuity element are used while the fluid pressure is evaluated at the center of the cells. We solve the coupling of elasticity and lubrication flow in a fully implicit manner. We use the universal HF tip asymptotic solution originally derived for the isotropic case (Garagash *et al.*, 2011; Dontsov and

Peirce, 2015) but using for the proper elastic modulus E'_α as function of the local fracture front propagation direction. It is important to note that, for the anisotropy, the near-tip plane strain modulus and possibly material toughness depends on the local propagation direction. As a result, an additional iterative loop is required in the implicit level set algorithm in order to converge on the local propagation direction (at each ribbon cells). More details are given in Zia *et al.* (2018).

The discretization of the elasticity equation (Eq.1) use the piece-wise rectangular displacement discontinuity element for transverse isotropy (see e.g. Pan *et al.* (2014)).

6. NUMERICAL RESULTS

6.1. Elliptical HF benchmark

We first benchmark our numerical solver with the analytical solution derived above for an elliptical HF. It is important to note that in order for the fracture to be elliptical, the material fracture toughness must follow Eq. (20). We therefore use such type of toughness anisotropy in our numerical simulation and compare the numerical and analytical width, pressure, and radius evolution with time.

We set the value of the toughness and elasticity ratios to: $\kappa^{-1} = \beta = 1.2$ such that the elliptical fracture aspect ratio is $b(t)/a(t) = 0.47$. The fracture is initialized as an ellipse of ratio 0.5 (slightly off the correct solution). The computational domain is divided into 150 cells along e_1 and 100 cells along e_3. Figs. 3,4 and 5 display the numerical (black dots) and analytical (green solid line) solution for the self similar dimensionless width profile as well as the evolution of dimensionless radius and dimensionless maximum width and pressure with time. The analytical solution for radius, width and pressure are reported in Eqs. (23), (11) and (22) respectively. We plot also the analytical results in dot-dashed line for the case of planar fracture propagating in isotropic media ($\kappa^{-1} = \beta = 1$).

The dimensionless width w/W_k along the major axis e_1 and the minor axis e_3 are displayed in Fig. 3. We can observe that the numerical results matches very the elliptical HF analytical solution derived above. The extent of the major axis $[-a/L_k, a/L_k]$ (top-figure) and the minor axis $[-b/L_k, b/L_k]$ (bottom-figure) are depicted from the width profiles which depart from the value $w = 0$ at the fracture tip $x_1 = \pm a$ and $x_3 = \pm b$. The fracture width extent is wider along the major axis than the minor axis with the same maximum width value at the center. The fracture width shape for the isotropic case (dot-dashed line) does not predict the anisotropic width profiles.

We scale the time by a a dummy characteristic time t_k corresponding to the time required to get a unit fracture length: $L_k(t_k) = 1$, and similarly for the width by $w(t)/W_k(t_k)$, the net pressure $p(t)/P_k(t_k)$, and the semi-axis $a(t)/L_k(t_k)$ and $b(t)/L_k(t_k)$. We can observe from figures (Figs. 4 and 5) that our numerical simulation follow accurately the analytical solution over more than four decades of time. The HF growth evolves self similarly with the same power law of time as for the isotropic case: $2/5$ for the radius, $1/5$ for width and $-1/5$ for the pressure. A maximum relative error on the fracture radius is estimated to 5% (Fig. 4-bottom) with respect to the elliptical toughness dominated HF solution.

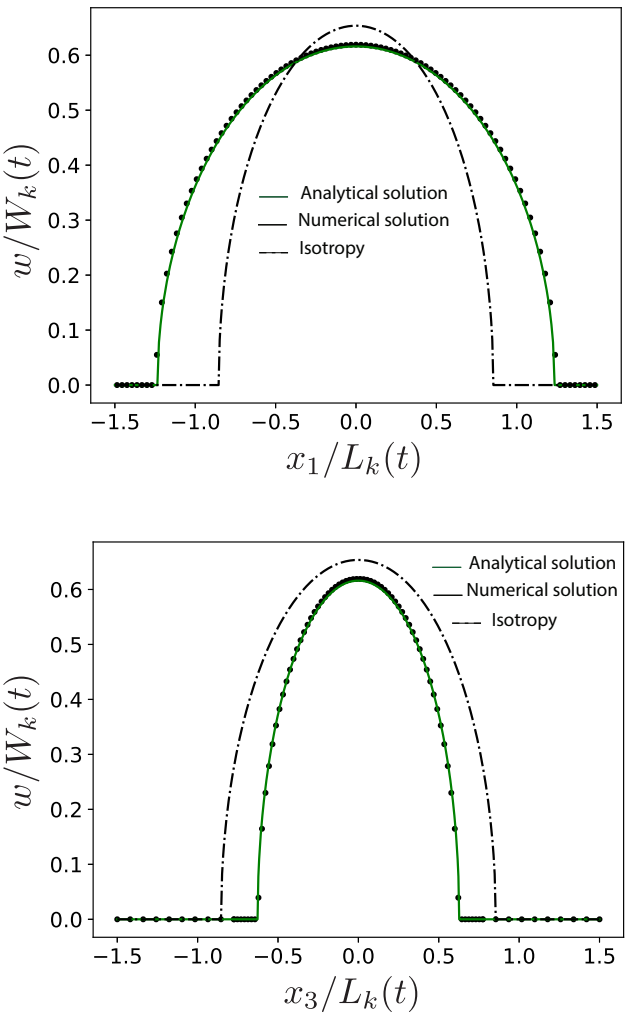

Fig. 3: Toughness dominated elliptical HF: self similar width profiles $w(t)/W_k(t_k)$ along the major axis e_1 (top-figure) and the minor axis e_3 (bottom-figure) for $\kappa^{-1} = 1.2$, $\beta = 1.2$, $\varepsilon = 0.3$, $\delta = 0.2$, and $C_{13}/C_{11} = 0.5$.

6.2. Isotropic toughness

We now study the effect of the dimensionless elastic anisotropy ratio β. We relax the assumption of an elliptical fracture and consider the case of an isotropic material toughness ($K_{Ic}(\alpha) = K_{Ic} \;/\; \kappa^{-1} = 1$). We perform a series of fracture propagation simulations for different TI parame-

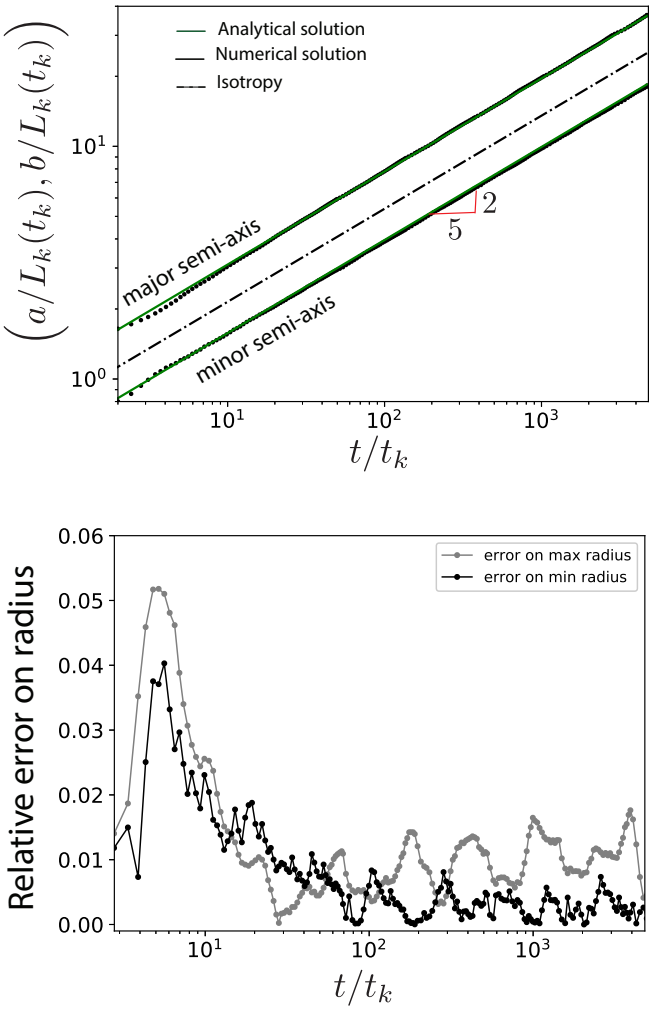

Fig. 4: Toughness dominated elliptical HF: Dimensionless major $a(t)/L_k(t_k)$ and minor $b(t)/L_k(t_k)$ semi axis in log-log scale in the top-figure, the relative error with respect to the analytical solution is shown in the bottom-figure. Case for $\kappa^{-1} = 1.2$, $\beta = 1.2$, $\varepsilon = 0.3$, $\delta = 0.2$, and $C_{13}/C_{11} = 0.5$.

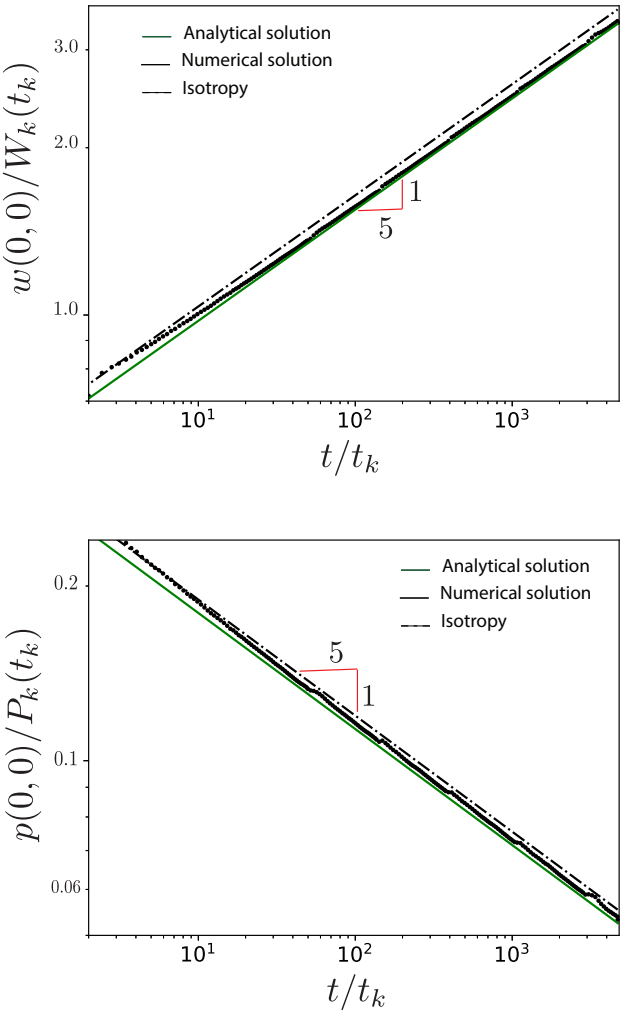

Fig. 5: Toughness dominated elliptical HF: dimensionless width $w(0,0)/W_k(t_k)$ (top-figure) and pressure $p(0,0)/P_k(t_k)$ (bottom-figure) at the injection point function of dimensionless time t/t_k in log-log scale. Case for $\kappa^{-1} = 1.2$, $\beta = 1.2$, $\varepsilon = 0.3$, $\delta = 0.2$, and $C_{13}/C_{11} = 0.5$.

ters with the base dimensionless elastic parameters ($\varepsilon = 0.3$, $\delta = 0.2$, and $C_{13}/C_{11} = 0.5$), varying only β. Here again after a short initial transient during which the fracture shape evolves from the initial solution (taken here as a radial), the fracture propagation exhibit a self-similar nature.

The self similar footprint and width profiles $w(t)/W_k(t_k)$ along the major and the minor axis e_1 and e_3 are displayed on Figs. 6-top and 7 respectively; while, the corresponding time dependence dimensionless semi-axis $(a(t), b(t))$ are displayed in Fig. 6-bottom. We scale the fracture radius with $L_k(t_k) = 1$ and time t here again with t_k (Fig. 6-bottom).

We report also in Fig. 6-top the numerical results obtained using the approximation E'_{app} (Eq. (10)) instead of the exact expression for the near tip plane-strain modulus. We can directly observe that the fracture deviates from the radial shape as it is the case for the isotropy. However, it does not exactly fit within an elliptical shape. The elongation of the fracture footprint b/a increases linearly with β^{-2} as shown in Fig.6-top-inset, a direct result from the toughness asymptote (Eq. (9)), where at the fronts located at the arrester and divider directions: $\sqrt{\dfrac{\delta x_3}{\delta x_1}} = \beta^{-1}\dfrac{w(\delta x_3)}{w(\delta x_1)}$. This is also the case for the elliptical shape (see Eq. (21)).

The numerical results, obtained using E'_{app} as the near-tip plane-strain modulus underestimate the fracture footprint aspect ratio - especially for large β. As an illustration, for $\beta = 2$, the ratio of the minor and major axis obtained using E'_{app} is equal to 0.59, whereas it is estimated as 0.32 when using the exact expression of E'_{α} in the near tip plane strain modulus. For smaller anisotropy, i.e: $\beta = 1.2$, the two near-tip plane strain modulus are relatively similar (see Fig.2.a), and as a results the two fracture footprints obtained numerically match very well for β close to unity (weak anisotropy).

For a given set of elastic parameters, the dimensionless fracture radius along the major axis e_1 and minor axis e_3 (Fig. 6-bottom) evolves as the $2/5$ power law of the time as expected from scaling arguments (see Tab.1). We also observe that larger anisotropy (higher value of β) results in a significantly lower fracture aspect ratio γ. This result is expected as the local growth of the fracture is governed mostly by the value of the near-tip elastic modulus magnitude for given isotropic fracture toughness (see Eq. (9)).

The self similar width profiles along the major and the minor axis are shown in Fig. 7. For different values of β, the self similar width profiles $w(t)/W_k(t_k)$ follows the evolution of the profiles of footprint, i.e: larger elongation on the fracture footprint corresponds to larger maximum opening along both minor and major axis. The fracture width is thiner along the minor axis. The width profiles also differ significantly from the isotropic case.

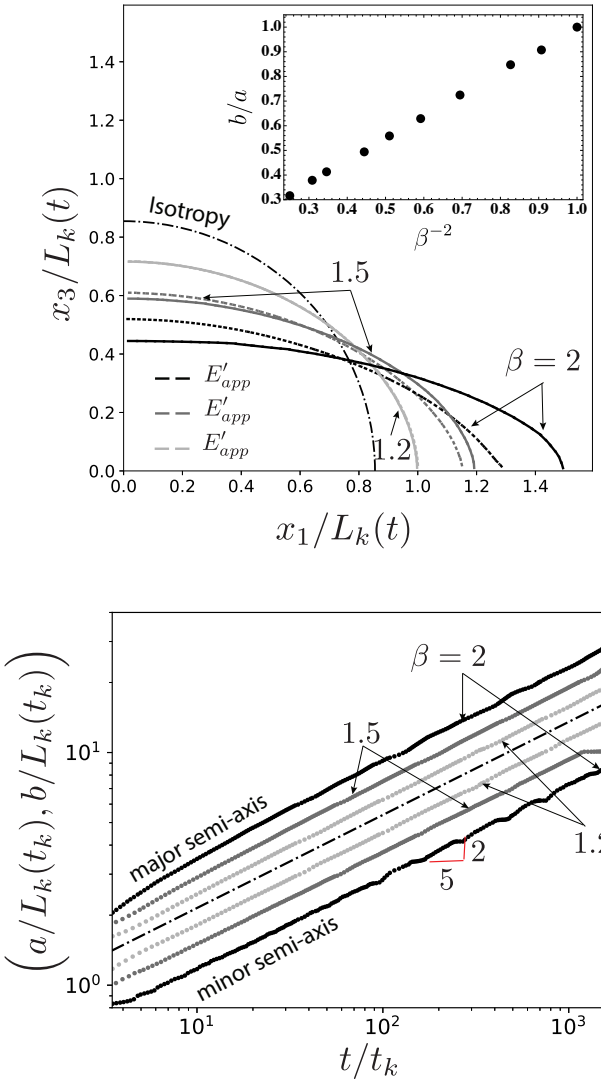

Fig. 6: Isotropic toughness / TI Elasticity: Self similar footprint (top-figure) obtained using the exact near-tip plane strain modulus E'_{α} (solid line) and the approximation E'_{app} (dashed lines), and time evolution of the dimensionless major $a(t)/L_k(t_k)$ and minor $b(t)/L_k(t_k)$ semi axis (bottom-figure). Effect of different $\beta = \{1.2, 1.5, 2\}$ with: $\varepsilon = 0.3$, $\delta = 0.2$, and $C_{13}/C_{11} = 0.5$.

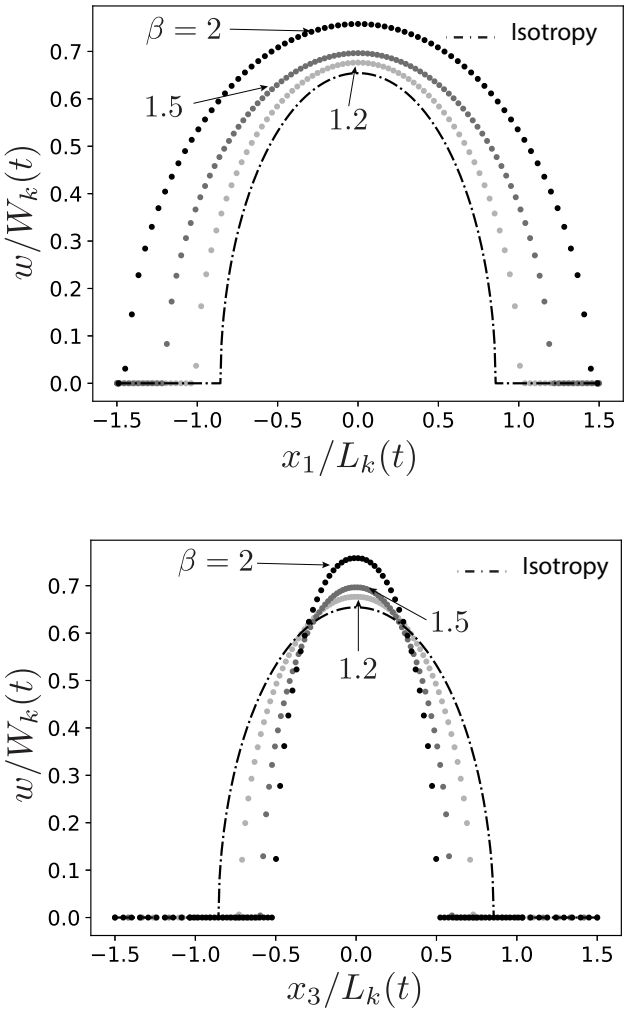

Fig. 7: Isotropic toughness / TI Elasticity: Self similar solution for width profiles $w(t)/W_k(t_k)$ along the major axis e_1 (top-figure) and the minor axis e_3 (bottom-figure) for different $\beta = \{1.2, 1.5, 2\}$ with $\varepsilon = 0.3$, $\delta = 0.2$, and $C_{13}/C_{11} = 0.5$.

7. SELF-SIMILAR FRACTURE SHAPE: FULLY COUPLED VERSUS APPROXIMATED SOLUTIONS

As previously mentioned, at large time, the hydraulic fracture propagates in toughness dominated regime (where the net pressure is spatially uniform) - and reach a self-similar shape (see section 6). We have reported in section 6.2 the influence of elastic anisotropy (assuming isotropic toughness) on such a shape - and observed that anisotropy promotes fracture elongation but the shape does not match exactly an elliptical shape. It is therefore interesting to further compare our numerical results obtained by solving the fully coupled hydraulic fracture problem without any priori constraints on the fracture shape with a simple shape adaptation scheme solely based on the assumption of an elliptical fracture (Laubie and Ulm, 2014).

The crack shape adaptability scheme proposed by Laubie and Ulm (2014) consists in numerically obtaining γ for a given set of elastic parameters such that either the stress intensity factor or the local energy release rate along the fracture front of an *elliptical* uniformly pressurized fracture is constant - therefore corresponding to an assumption of isotropic material toughness or isotropic fracture energy respectively.

The hypothesis of an isotropic material toughness requires that the stress intensity factor for the uniformly pressurized elliptical crack (14) is constant all around the fracture front. For a given set of elastic parameters, one can therefore obtain the most suitable fracture aspect ratio by numerically minimizing the relative difference of K_I at different angles along the elliptical front:

$$\gamma = \min_{\gamma} \left(\sum_{i=1}^{N_\theta} \frac{K_I(\gamma,\beta,\theta_i) - K_I(\gamma,\beta,0)}{K_I(\gamma,\beta,0)} \right) \tag{24}$$

where we discretize the interval $[0, \pi/2]$ in $N_\theta = 20$ values of θ_i the polar angle (13) parametrizing the crack front. Note that K_I is also function of ε, δ and C_{13}/C_{11}.

One can perform a similarly scheme assuming that the local energy release rate $g = \dfrac{K_I^2}{E'_\alpha}$ is constant all along the front - isotropic critical fracture energy assumption. Similarly, again under the assumption of an elliptical shape, one can perform a minimization of the variation of g along the front as function of the aspect ratio γ:

$$\gamma = \min_{\gamma} \left(\sum_{i} \frac{g(\gamma,\beta,\theta_i) - g(\gamma,\beta,0)}{g(\gamma,\beta,0)} \right). \tag{25}$$

Moreover in both cases, one can either use the exact expression of the near-time plane-strain modulus E'_α (appearing in the expression of the local SIF (14) and energy release rate), or the approximation E'_{app} (as done by Laubie and Ulm (2014)).

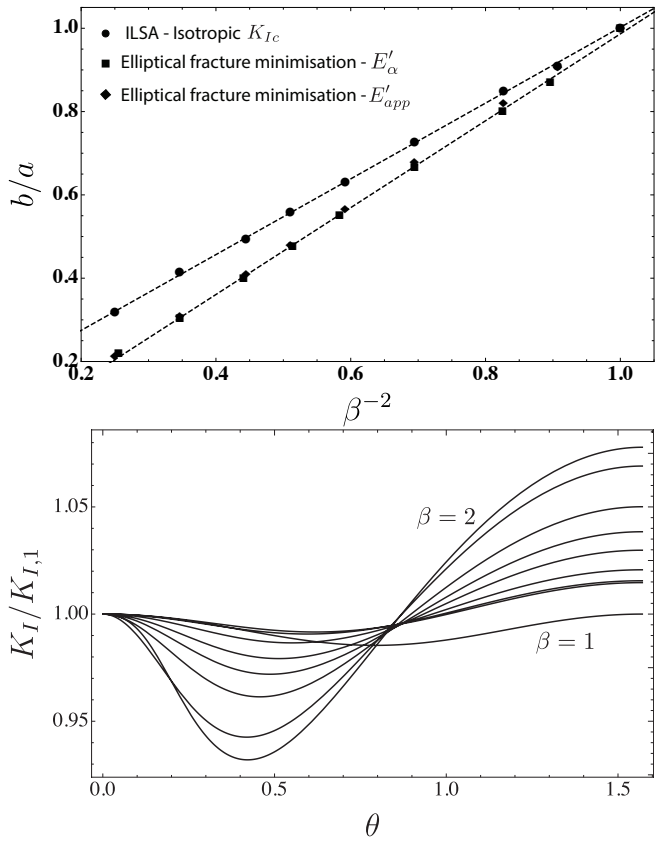

Fig. 8: Top: Comparison of the fracture aspect ratios b/a obtained from the numerical solution (black dot), the SIF minimization criteria using E'_α (black square) or the approximation E'_{app} (black diamond) for the near tip plane strain modulus. Results for different $\beta^{-2} = \{1, 1.05, 1.1, 1.2, 1.3, 1.4, 1.5, 1.7, 2\}^{-2}$ with $\varepsilon = 0.3$, $\delta = 0.2$, and $C_{13}/C_{11} = 0.5$ for all cases. Bottom: corresponding scaled stress intensity factor $K_I/K_{I,1}$ function of θ.

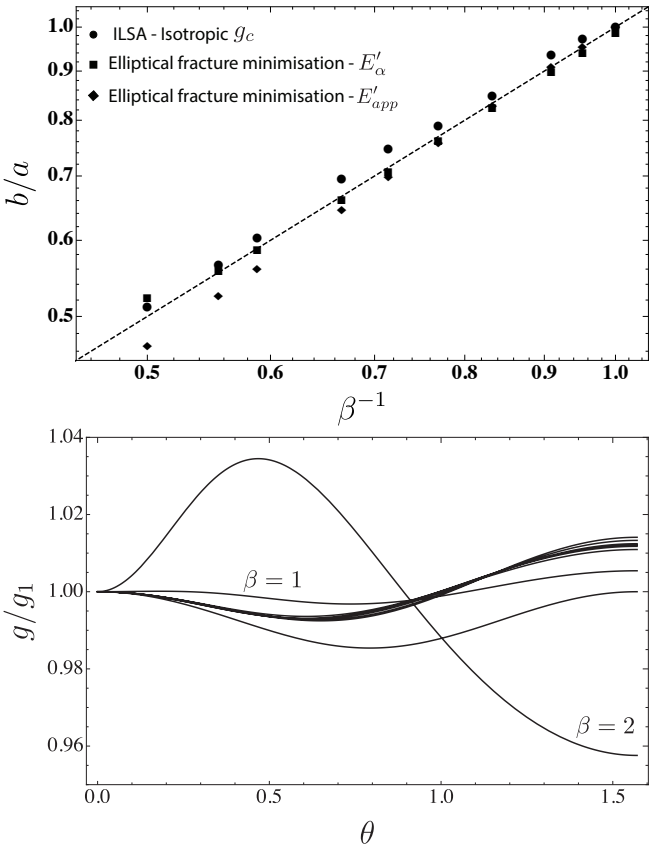

Fig. 9: Top: Comparison of the fracture aspect ratios b/a obtained from the numerical solution (black dot), the fracture energy minimization criteria using E'_α (black square) or the approximation E'_{app} (black diamond) for the near tip plane strain modulus. Results for different $\beta^{-1} = \{1, 1.05, 1.1, 1.2, 1.3, 1.4, 1.5, 1.7, 2\}^{-1}$ with $\varepsilon = 0.3$, $\delta = 0.2$, and $C_{13}/C_{11} = 0.5$ for all cases. Bottom: corresponding scaled local energy release rate g/g_1 function of θ.

7.1. Hypothesis of isotropic toughness

Fig. 8-top represents the ratio b/a as function of β obtained by minimizing the variation of stress intensity factor along an elliptical fracture front - either using E'_α or its approximation E'_{app} as the near tip plain strain modulus. The numerical results obtained without the constraint of an elliptical fracture are also reported as black dots. For small values of β ($\beta^{-1} > 0.8$) the results obtained with the assumption of an elliptical fracture and the numerical ones (unconstrained) agrees well with the same slope function of β^{-2} ($\gamma = 1.04\beta^{-2}$). When the anisotropy increases ($\beta^{-1} < 0.8$), the results obtained via minimization of variation of K_I for an elliptical crack starts to significantly differ form the numerical prediction of the fracture front for which $\gamma = 0.9\beta^{-2}$. The relative error between the two estimations exceeds 30% for the case of high anisotropies ($\beta^{-1} < 0.3$). Moreover as expected, the stress intensity factor along the elliptical crack front are not uniform even at the optimal γ value obtained -see Fig. 8-bottom for the dimensionless SIF $K_I/K_{I,1} = K_I(\theta)/K_I(\theta = 0)$ along the front. The non-uniformity reaches 5% for the largest elastic anisotropy.

7.2. Hypothesis of isotropic fracture energy

Similarly than before, we perform HF numerical simulations imposing an isotropic fracture energy g_c for different elastic anisotropy. We compare our fully coupled numerical results (without any constraint on the fracture shape) and the results obtain by minimizing the non-uniformity of g along the front of an elliptical crack. Using the approximation E'_{app} or the complete modulus E'_α, the elliptical crack shape adaptability follows relatively well our numerical results except the case when $\beta^{-1} < 0.6$ (see Fig. 9-top). We found that the crack shape using the energy criteria scales as ratio β^{-1} which is expected as: $g(\theta = 0)/g(\theta = \pi/2) = \beta^{-1}$.

One can also note that the variation of the scaled energy release rate $g/g_1 = g(\theta)/g(\theta = 0)$ along the front of the elliptical crack at the optimal γ appears more uniform (see Fig. 9-bottom). The spatial variation is only of a few percent for the largest value of $\beta = 2$ ($\beta^{-1} = 0.5$).

8. CONCLUSIONS

In this paper, we have presented a numerical solver to simulate the growth of a planar 3D hydraulic fracture propagating normal to the plane of isotropy of a transversely isotropic elastic rock. Our numerical solver was validated against an analytical solution in toughness dominated regime for a special case of toughness anisotropy leading to an elliptical fracture. The main conclusions of this study are the following.

- Both elastic and toughness anisotropy tends to elongate the fracture in the horizontal direction in the most common settings of sedimentary basins.
- Only a very peculiar form of toughness anisotropy (Eq. (20)) leads to an *exactly* elliptical shape - which is highly unlikely for any material.
- The effect of the anisotropy of elasticity and toughness on fracture elongation is compounded when $\kappa = K_{Ic,1}/K_{Ic,3}$ is below 1.
- Under the hypothesis of isotropic toughness, the aspect ratio obtained numerically (without constraining the fracture to be elliptical) is proportional to $\beta^{-2} = (E'_1/E'_3)^2$, i.e. $\gamma \approx 0.9\beta^{-2}$, but the fracture(s) are not *exactly* elliptical. Minimizing the SIF variation along the front of an elliptical fracture (a strong assumption) provides a more elongated fracture shape and the SIF remains non-uniform confirming that under such assumption the fracture can not be exactly elliptical.
- Under the hypothesis of an isotropic critical fracture energy, the aspect ratio obtained numerically (without constraining the fracture to be elliptical) is proportional to $\beta^{-1} = E'_1/E'_3$, i.e. $\gamma \approx \beta^{-1}$. Here the minimization of the local energy release rate along the front of an elliptical fracture provides similar results, although the local energy release rate is not exactly uniform along the front. Here again under such an assumption the fracture can not be exactly elliptical.

Acknowledgments This work was funded by the Swiss National Science Fondation under grant #160577.

REFERENCES

1. Barnett, D. and Asaro, R., 1972. The fracture mechanics of slit-like cracks in anisotropic elastic media, *Journal of the Mechanics and Physics of Solids*, 20 (6), 353–366.
2. Bonnet, M., 1999. *Boundary integral equation methods for solids and fluids*, vol. 34, Springer, wiley-blackwell ed.
3. Detournay, E., 2016. Mechanics of hydraulic fractures, *Annual Review of Fluid Mechanics*, 48, 311–339.
4. Dontsov, E. and Peirce, A., 2015. *A non-singular integral equation formulation to analyse multiscale behaviour in semi-infinite hydraulic fractures*, vol. 781, Cambridge University Press.
5. Eshelby, J., Read, W., and Shockley, W., 1953. Anisotropic elasticity with applications to dislocation theory, *Acta metallurgica*, 1 (3), 251–259.
6. Fabrikant, V., 2011. Non-traditional crack problem for transversely-isotropic body, *European Journal of Mechanics-A/Solids*, 30 (6), 902–912.
7. Garagash, D., 2009. Scaling of physical processes in fluid-driven fracture: perspective from the tip, 91–100.
8. Garagash, D., Detournay, E., and Adachi, J., 2011. Multiscale tip asymptotics in hydraulic fracture with leak-off, *Journal of Fluid Mechanics*, 669, 260–297.
9. Hills, D., Kelly, P., Dai, D., and Korsunsky, A., 1996. *Solution of crack problems: the distributed dislocation technique*, *Solid Mechanics and its Applications*, vol. 44, Kluwer Academic Publ.
10. Hirth, J.P. and Lothe, J., 1982. *Theory of dislocations*, John Wiley and Sons, Inc.
11. Hoenig, A., 1978. The behavior of a flat elliptical crack in an anisotropic elastic body, *International Journal of Solids and Structures*, 14 (11), 925–934.
12. Kanaun, S., 2007. An elliptical crack in an anisotropic elasic medium subjected to a constant external field, *International Journal of Fracture*, 148 (1), 95–102.
13. Keer, L. and Lin, W., 1990. Analysis of cracks in transversely isotropic media, *in: Micromechanics and Inhomogeneity*, Springer, 187–195.
14. Laubie, H. and Ulm, F., 2014. Irwin's conjecture: Crack shape adaptability in transversely isotropic solids, *Journal of the Mechanics and Physics of Solids*, 68, 1–13.
15. Lin, W. and Keer, L., 1989. Three-dimensional analysis of cracks in layered transversely isotropic media, 424 (1867), 307–322.
16. Madyarova, M. and Detournay, E., 2003. *Fluid-driven penny-shaped fracture in permeable rock*, Master's thesis, University of Minnesota.
17. Mogilevskaya, S., 2014. Lost in translation: crack problems in different languages, *International Journal of Solids and Structures*, 51 (25-26), 4492–4503.
18. Pan, E., Yuan, J., Chen, W., and Griffith, W., 2014. Elastic deformation due to polygonal dislocations in a transversely isotropic half-space, *Bulletin of the Seismological Society of America*, 104 (6), 2698–2716.
19. Pan, Y. and Chou, T., 1976. Point force solution for an infinite transversely isotropic solid, *Journal of Applied Mechanics*, 43 (4), 608–612.
20. Peirce, A. and Detournay, E., 2008. An implicit level set method for modeling hydraulically driven fractures, *Computer Methods in Applied Mechanics and Engineering*, 197 (33), 2858–2885.
21. Savitski, A. and Detournay, E., 2002. Propagation of a penny-shaped fluid-driven fracture in an impermeable rock: asymptotic solutions, *International Journal of Solids and Structures*, 39 (26), 6311–6337.
22. Stroh, A., 1958. Dislocations and cracks in anisotropic elasticity, *Philosophical magazine*, 3 (30), 625–646.

23. Voigt, W., 1928. *Lehrbuch der kristallphysik*, vol. 962, Teubner Leipzig.

24. Zia, H., Lecampion, B., and Zhang, W., 2018. Impact of the anisotropy of fracture toughness on the propagation of planar 3d hydraulic fracture, *International Journal of Fracture*, 211 (1-2), 103–123.